WILEY | Hindawi

Research Article

Characterization of Viscoelastic Properties Considering the Nonrelaxation for Filled Rubber

Xinyi Lin [iD],[1] Mengxi Huang,[2] Yang Wang,[1] and Ziran Li [iD][1]

[1]*CAS Key Laboratory of Mechanical Behavior and Design of Materials, Department of Modern Mechanics, University of Science and Technology of China, Hefei, Anhui 230027, China*
[2]*School of Civil Engineering and Architecture, Nanchang University, Nanchang, Jiangxi 330031, China*

Correspondence should be addressed to Ziran Li; lzr@ustc.edu.cn

The influence of nonrelaxation on the Payne effect of carbon black-filled rubber is studied. The prestrain is introduced in the Kraus model in the form of exponential growth. Combined with studies of temperature correlations, an explicit model for predicting the Payne effect at different prestrains and temperatures is developed. Dynamic mechanical analyses are performed to determine model parameters and validate the proposed model. To further verify the proposed model, the heat buildup of rubber columns under dynamic tensile load is tested and simulated. The comparison between simulated and measured data shows that the simulation considering nonrelaxation is more accurate than without considering. With the increase of prestrain, the accuracy of considering nonrelaxation becomes more obvious.

1. Introduction

Carbon black-filled rubber is widely used as the main material of tire and rubber inflatable springs. For safety and economy, it is necessary to fully study the dynamic mechanical properties of carbon black-filled rubber, which determine the loss characteristics of the rubber. On account of nonlinear viscoelasticity, the dynamic moduli are affected by strain amplitude, temperature, frequency, and prestrain.

Payne found that the dynamic moduli of carbon black-filled rubber change with strain amplitude, and this strain amplitude correlation is also known as the Payne effect [1, 2]. Some constitutive models have been put forward to characterize the Payne effect well [3–6]. Among them, the Kraus model [7] is the famous phenomenological model to represent the Payne effect on a physical level, which has been modified by Ulmer [8]. Dean et al. [9] found that the dynamic modulus of carbon-filled rubber decreases with increasing temperature. In the process of establishing thermomechanically consistent constitutive models, Lion et al. [10] put forward the concept of hybrid-free energy density. This concept optimizes the characterization of the properties of thermomechanical coupling materials under complex mechanical states. Hu et al. [11] combined the Kraus model with the Williams–Landel–Ferry equation [12] and derived a model to predict the dynamic modulus at various temperatures. Lion [13] and Vieweg et al. [14] found that the dynamic modulus of carbon-filled rubber decreases with increasing temperature and increases with rising frequency. Delattre et al. [15] present a constitutive model of filled rubber, which can consider special phenomena of dynamic loads at different temperatures, such as the Payne effect and frequency dependency. Delattre's model can adapt to the corresponding frequency and temperature range by adjusting the number and parameters of viscous stresses. Luo et al. [16] considered that the maximum loss modulus in the Kraus model is linearly correlated with frequency; the suggested model can predict the Payne effect with varying frequency well. The viscoelastic properties of filled rubber change with relaxation state [17, 18]. Dutta and Tripathy [17] observed that the storage and loss moduli of carbon black-filled rubber have an obvious minimum with increasing prestrain. However, Lion [13] observed that the loss modulus decreases with the increase of prestrain. It can be seen that the influence of prestrain on viscoelasticity is

complex. Wollscheid and Lion [19] studied the significant influence of large prestrain on the material behavior at small dynamic strains where dynamic moduli are nearly constant. By linearizing Simo's model [20] and introducing octahedral shear strain as a prestrain correction factor, Kim and Youn [21] derived a K–Y model that can well describe the dynamic modulus variation with prestrain under small vibration.

In the process of tire research and development, the tire steady-state temperature field needs to be simulated [22–24]. Research on dynamic characteristics of tire compounds is the key to the simulation of the tire temperature field. The frequency range corresponding to the traveling speed of the tire is 0–30 Hz. When the temperature is above 60°C, the dynamic modulus of the tire compound has little change in the frequency range of 0–30 Hz [25]. For pneumatic tires, tire rubber obviously experiences dynamic load in a nonrelaxed state, which means that the influence of prestrain and Payne effect on viscoelastic characteristics cannot be ignored [26, 27]. In addition, the temperature rise caused by the viscoelastic loss of tire rubber also affects the viscoelastic property [28, 29]. However, we have not found a model that can consider the influence of both prestrain and temperature on the Payne effect in the literatures.

The aim of this paper is to propose an explicit model to predict the Payne effect of carbon black-filled rubber under different prestrains and temperatures. The Kraus model considering prestrain and temperature (KMPT) is derived from the introduction of prestrain in the Kraus equation, combined with previous studies about the temperature dependence of the Payne effect. A good agreement between the KMPT and prestrain sweeps data is achieved. To further verify the KMPT, the heat buildup (HBU) of dumbbell-shaped rubber columns under dynamic tensile load is tested and simulated. Besides, the HBU simulations considering nonrelaxation are compared with those without considering.

2. Dynamical Mechanical Analysis (DMA)

The base of the material (tire body compound) is synthetic rubber; the filler is carbon black and other additives. However, the specific recipe cannot be listed due to confidentiality. The DMA test was performed on a dumbbell specimen with a thickness of 2 mm. The geometry and the size of specimens can be seen in Figure 1.

The DMA tests are divided into two parts: prestrain correlation test and temperature correlation test, and performed by a dynamic mechanical analyzer (DMA + 2000, produced by Metravib of France) working in tensile mode. The test conditions are determined by the simulation results of radial tire deformation and related literatures [26, 30, 31]. In the prestrain correlation test, prestrain sweeps were conducted under the prestrain ranged from 8% to 70%, various sinusoidal strain amplitude, i.e., 1%, 2%, 3%, 5%, 7%, a frequency of 10 Hz, and a fixed temperature of 25°C. In the temperature correlation test, dynamic strain amplitude sweeps were conducted under various temperatures, i.e., 25, 50, 75, 100, and 125°C, and the amplitude ranged from 0.01% to 10%, a frequency of 10 Hz, and a fixed prestrain of 15%. Mullins
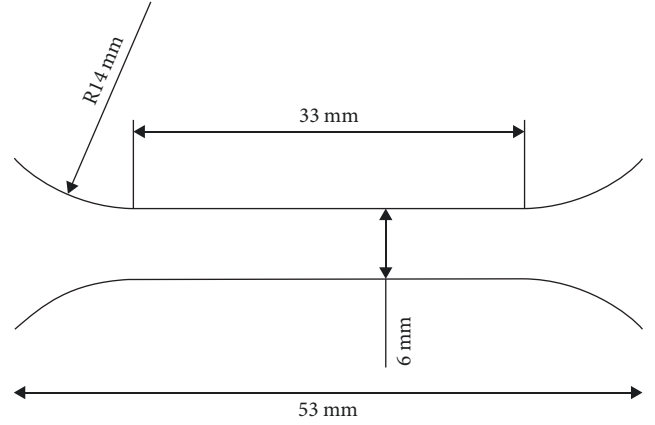

Figure 1: Dimensions of dumbbell specimen.

effect of samples was excluded primarily by cycling the tensile load ten times with the maximum strain and the frequency of 10 Hz.

3. Characterization of Dynamic Modulus

When studying the temperature correlation of material parameters, the Arrhenius equation is often used [32, 33], which is the exponential form of temperature [11, 34]. So, to characterize the temperature dependence of the Payne effect, the following models are proposed:

$$E'(\varepsilon_0, T) = E'_\infty(T) + \frac{\Delta E'(T)}{1 + (\varepsilon_0/\varepsilon_c')^{2m'}}, \tag{1}$$

$$E''(\varepsilon_0, T) = E''_\infty(T) + \frac{\Delta E''(T)\varepsilon_0^{m''}}{1 + (\varepsilon_0/\varepsilon_c'')^{2m''}}, \tag{2}$$

$$Y(T) = A_1 \cdot \exp(-T/B_1) + Y_1, \tag{3}$$

where $Y(T)$ represents $E'_\infty(T)$, $\Delta E'(T)$, $E''_\infty(T)$, and $\Delta E''(T)$. T is the temperature. A_1, B_1, and Y_1 are the temperature-dependent coefficient. ε_0 is the dynamic strain amplitude. ε_c' is the characteristic value of the strain amplitude at which the storage modulus E' reached its peak E'_m, ε_c'' is the characteristic value of the strain amplitude at which the loss modulus E'' reached its peak E''_m. When ε_c' and ε_c'' are different, the fitting effect of Kraus model will be better [8]. $\Delta E'$, $\Delta E''$, m', and m'' are material parameters. The parameters ε_c', m', ε_c'', and m'' are only related to the material types, as reported literatures [4, 35]. Equations (1)–(3) are applied to fit the temperature correlation experimental data, and the fitting results (Figures 2(b) and 3(b)) reveal that the change of the Payne effect with temperature can be well captured by exponential form.

Therefore, we further guess that the prestrain ε_s also has an exponential relationship with the parameters: E'_∞, $\Delta E'$, E''_∞, and $\Delta E''$, as Equation (6) shown. Based on this conjecture, we tried to fit the Payne effect data of the compound under different prestrains. It is found that the fit was good, as shown in Figures 2(a) and 3(a). Therefore, we proposed a
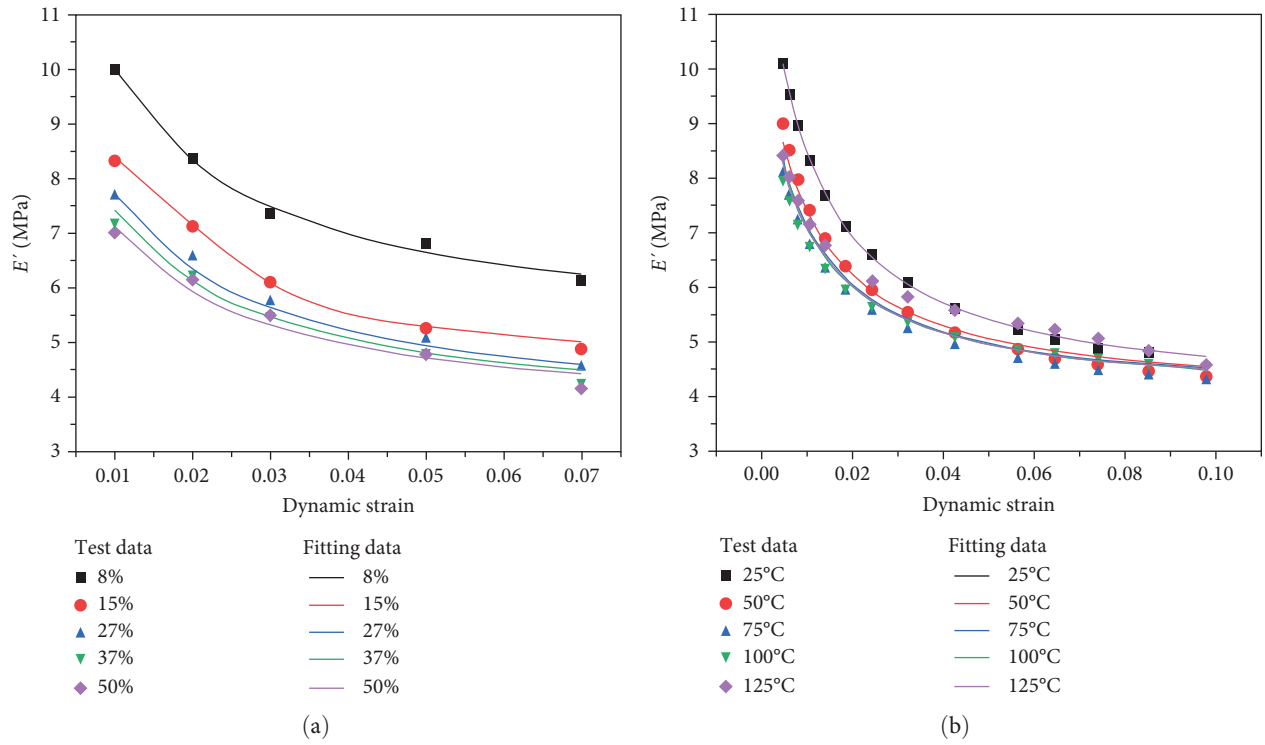
FIGURE 2: Storage modulus vs. dynamic strain: (a) different prestrains at temperature 25°C; (b) different temperatures at prestrain 15%.
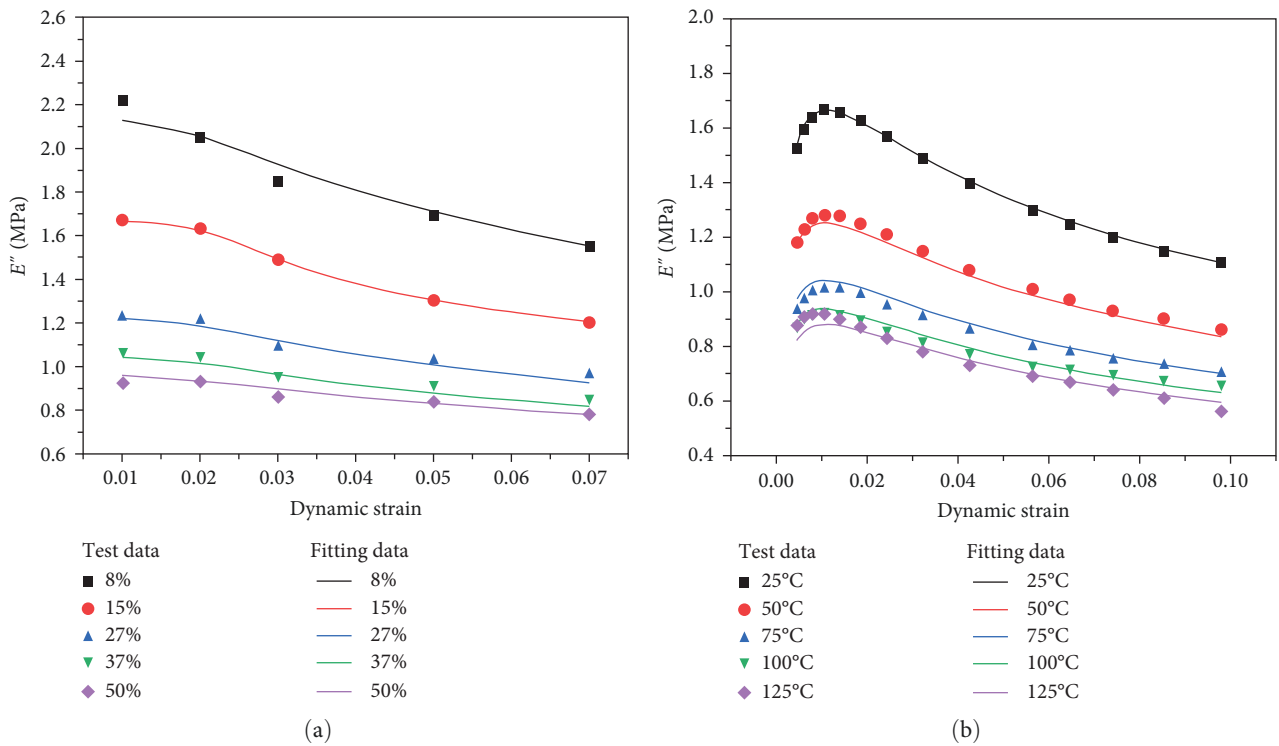

FIGURE 3: Loss modulus vs. dynamic strain: (a) different prestrains at temperature 25°C; (b) different temperatures at prestrain 15%.

TABLE 1: Determined coefficients and parameters.

	E'_∞ (MPa)	$\Delta E'$ (MPa)	E''_∞ (MPa)	$\Delta E''$ (MPa)
A_1	0.101	11.336	0.407	25.708
B_1	1.613	17.58	0.271	37.037
Y_1	3.979	5.923	0.0592	11.898
A_2	1.7	0.546	28.71	1.558
B_2	−0.053	−0.365	2.731	−0.188
Y_2	0.9	0.638	−29.331	0.3
	ε'_c	m'	ε''_c	m''
	0.0109	0.532	0.011	0.455

KMPT as follows:

$$E'(\varepsilon_0, T, \varepsilon_s) = E'_\infty(T, \varepsilon_s) + \frac{\Delta E'(T, \varepsilon_s)}{1 + (\varepsilon_0/\varepsilon'_c)^{2m'}}, \qquad (4)$$

$$E''(\varepsilon_0, T, \varepsilon_s) = E''_\infty(T, \varepsilon_s) + \frac{\Delta E''(T, \varepsilon_s)\varepsilon_0^{m''}}{1 + (\varepsilon_0/\varepsilon''_c)^{2m''}}, \qquad (5)$$

$$Y(T, \varepsilon_s) = [A_1 \cdot \exp(-T/B_1) + Y_1] \cdot [A_2 \cdot \exp(\varepsilon_s/B_2) + Y_2], \qquad (6)$$

where $Y(T, \varepsilon_s)$ represents $E'_\infty(T, \varepsilon_s)$, $\Delta E'(T, \varepsilon_s)$, $E''_\infty(T, \varepsilon_s)$, and $\Delta E''(T, \varepsilon_s)$. A_2, B_2, and Y_2 are the prestrain dependent coefficients. It should be noticed that the KMPT model is a purely phenomenological model, and hence, the above parameters have no direct link with the rubber microstructure features.

Because of the huge workload, the experimental conditions cannot consider the influence factors of prestrain and temperature simultaneously. There are two fitting sequences: temperature before prestrain (Figures 2 and 3) and prestrain before temperature (Figures S1 and S2 in supplementary materials, and fitting parameters are listed in Table S1). By comparing the fitting results of the two sequences, it is found that the fitting sequence has no influence on the fitting effect. The sequence that first fitting temperature data is picked.

The least square method is applied in the fitting process, which is done by MATLAB. The fitting process of the loss modulus is the same as that of the storage modulus. According to Equations (4) and (6), the temperature-dependent coefficients A_1, B_1, Y_1, and constants ε'_c, m' are determined by fitting the test data of the storage modulus E' vs. the dynamic strain amplitude ε_0 under five different temperatures. Meanwhile, the prestrain part: $[A_2 \cdot \exp(\varepsilon_s/B_2) + Y_2]$ is set to unity at the constant prestrain of 15%, i.e., $[A_2 \cdot \exp(0.15/B_2) + Y_2] = 1$. The "0.15" indicates the prestrain 15%, which is the constant prestrain set in the DMA temperature correlation test. In the same way, the prestrain dependent coefficients A_2, B_2, Y_2 are established at the constant temperature of 25°C, and they are determined by fitting the test data of the storage modulus E' vs. the dynamic strain amplitude ε_0 at five different prestrains. The determined coefficients and parameters are shown in Table 1. Comparison between the fitted and test data indicates that the Payne
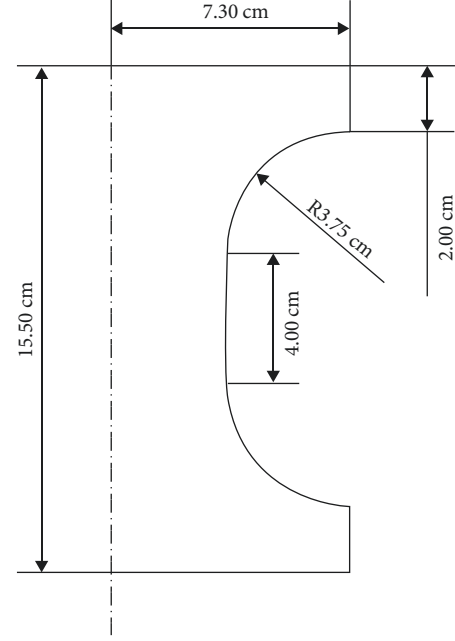

FIGURE 4: Size of the dumbbell-shaped rubber column.

effect at different prestrains and temperatures can be well predicted by the KMPT, which is demonstrated by Figures 2 and 3. KMPT is also applicable to other formulations of tire compounds (Figure S3 and S4 in supplementary materials); the corresponding parameters are shown in Table S2.

4. Experiment and Simulation of HBU

To further verify the KMPT, the HBU of rubber columns under different dynamic tensile loads was tested and simulated.

4.1. HBU Test. In the HBU test, the dumbbell-shaped rubber column was used, whose size is shown in Figure 4. The bottom of the dumbbell-shaped the rubber column was fixed and the top was subjected to sinusoidal displacement load d as expressed by Equation (7), as shown in Figure 5. Where d_s is the predisplacement load, d_0 is the dynamic tensile displacement amplitude, and f is the loading frequency ($f = 10\,Hz$). The three HBU test conditions of the rubber column are $d_s = d_0 = 2$, 4, and 5 mm, which was done by the universal testing instrument (Instron E3000). The room temperature was 22°C. The steady-state surface temperature of rubber columns was recorded by the infrared camera.

$$d = d_s + d_0 \sin(2\pi ft). \qquad (7)$$

4.2. Steady-State Temperature Field Simulation. Thermo-mechanical coupling simulation can be divided into two categories: decoupling [24] and full coupling [36]. Bazkiaei et al. [37] found that the decoupled method is better suited for steady-state simulation, and the coupled method is better
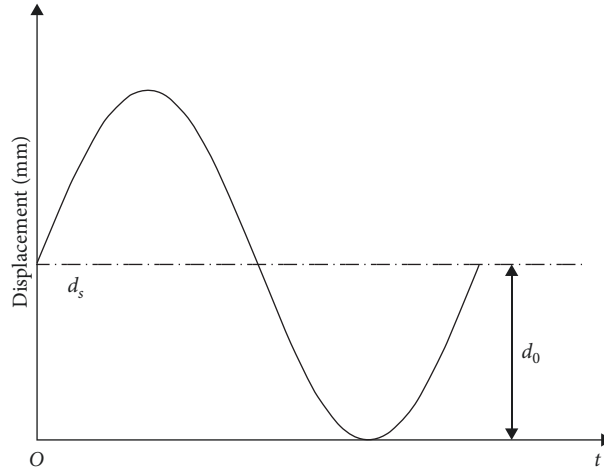
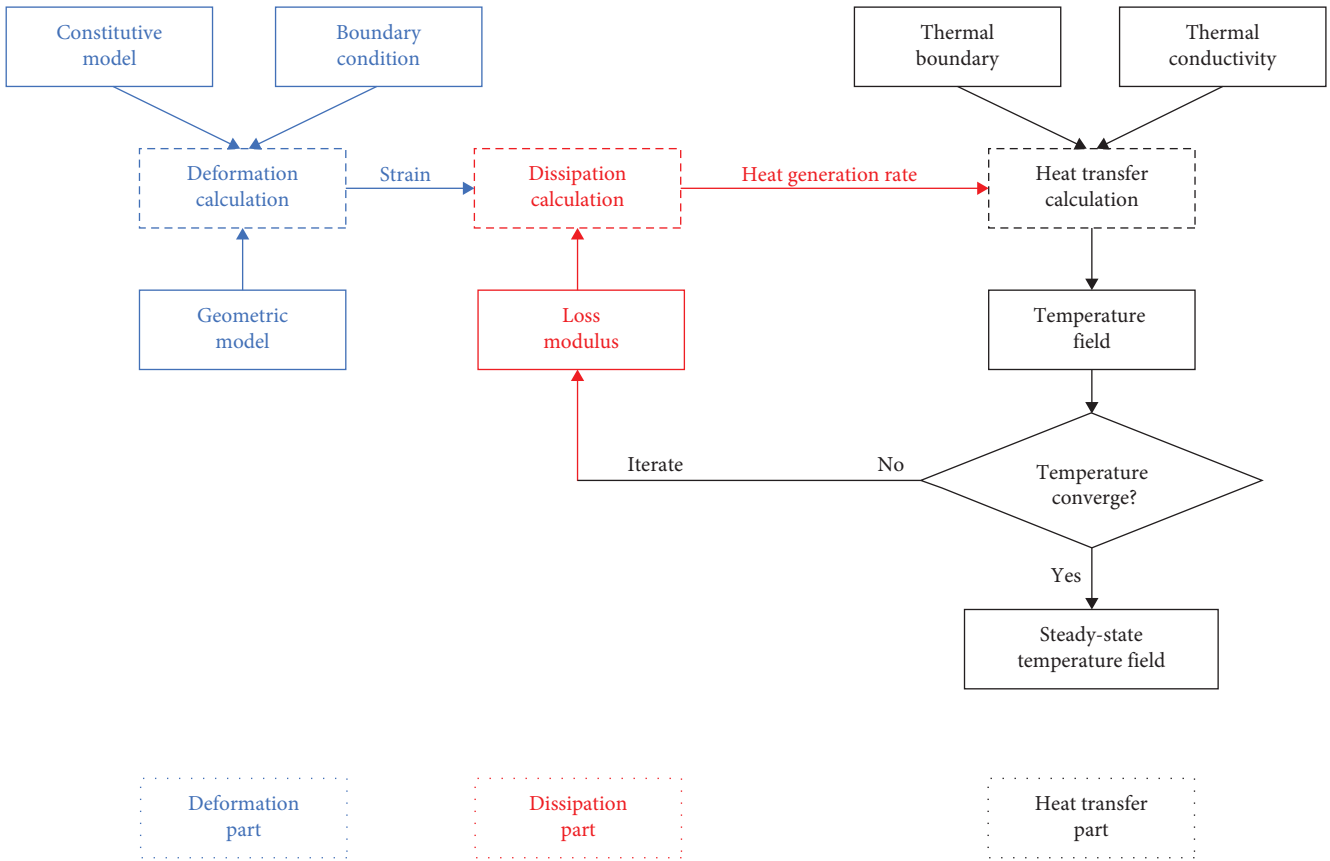FIGURE 5: Applied sinusoidal displacement load d.

FIGURE 6: Flowchart of decoupling strategy for thermomechanical coupling simulation.

suited for transient simulation. Because the steady-state temperature field was measured, the decoupling strategy is chosen in this section. We have done two simulations, one based on the KMPT (Equations (4)–(6)) and the other based on the Kraus model only considering temperature (Equations (1)–(3)).

The simulation consists of three parts [24, 38, 39]: deformation, dissipation, and heat transfer, as demonstrated in Figure 6. In the deformation part, only the deformation is concerned; usually, the hyperelastic model is adopted

[25, 39]. We choose the Yeoh constitutive model [40], as shown by Equation (8).

$$\psi = C_{10}(I_1 - 3) + C_{20}(I_1 - 3)^2 + C_{30}(I_1 - 3)^3, \quad (8)$$

where ψ is the strain energy function, I_1 is the first invariant of stretch. The Yeoh constitutive model material parameters
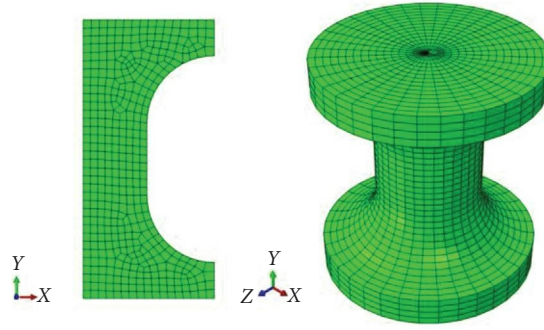
FIGURE 7: Mesh for deformation calculation (left: 2D axisymmetric elements, right: sweep elements).
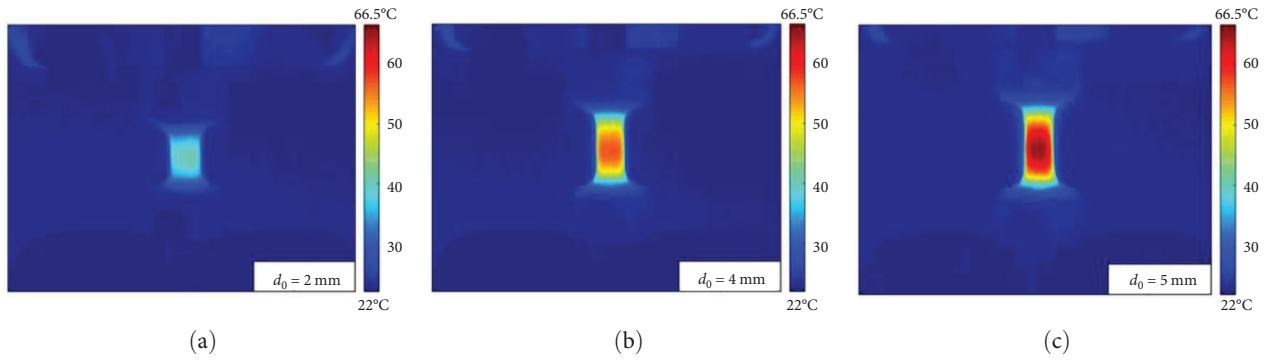

FIGURE 8: The infrared results of steady-state temperature filed on the rubber column surface: (a) $d_0 = d_s = 2$ mm; (b) $d_0 = d_s = 4$ mm; (c) $d_0 = d_s = 5$ mm.

of the tire body compound are provided in Table S3, and the fitting curves, along with the stress–strain experimental curves, are shown in Figure S5. The 2D axisymmetric elements (CAX4H) of ABAQUS are used, as shown in Figure 7. Due to the displacement control loading, the influence of temperature on deformation calculation is not considered. After the deformation calculation is completed, the strain history of the element is derived for the viscoelastic loss calculation in the dissipation analysis.

Dissipation calculation is done by the self-programmed program. In this part, under simple harmonic vibration with dynamic strain amplitude ε_0, the dissipation during one cycle per unit volume ξ_{loss} is calculated by Equation (9). Where ε_0 is derived from the strain history of each element, $E''(\varepsilon_0, T, \varepsilon_s)$ is obtained by the KMPT model. The resulting loss ξ_{loss} multiplied by the loading frequency f is the heat source of the element in the heat transfer analysis, as shown by Equation (10).

$$\xi_{\text{loss}} = \pi \varepsilon_0^2 E''(\varepsilon_0, T, \varepsilon_s), \tag{9}$$

$$\dot{q} = \xi_{\text{loss}} \cdot f. \tag{10}$$

The initial iteration temperature T_1 used to calculate the initial heat source $\dot{q}_1$ is 22°C (room temperature). The new temperature T_2 is obtained by bringing $\dot{q}_1$ into the heat conduction analysis. Bring T_2 into Equations (9) and (10)

to get the heat source $\dot{q}_2$ for the second iteration. If the calculated results of all node temperatures converge (i.e., steady-state), the temperature iteration stops. The convergent temperature distribution is the final steady-state temperature field. According to literatures [41, 42], the heat transfer coefficient of thermal boundary is considered to be a constant of 42 W m^{-2} K^{-1} for all HBU simulations, which is calculated from the experimental and numerical results at $d_0 = d_s = 2$ mm. Thermal parameters (Table S4) and more detailed thermal boundary conditions (Figure S6) are shown in supplementary materials. Therefore, only the simulation results under $d_0 = d_s = 4$ and 5 mm are demonstrated.

5. Results and Discussion

The interval from the beginning of loading to the steady state of the surface temperature field was 20 min. The infrared test results of the steady-state temperature filed on the rubber column surface are shown in Figure 8. The surface temperature variation with height is extracted from the infrared data, as shown in Figure 9. Figure 10 shows the starting position of the height. From Figures 8 and 9, we can see that the temperature field increases with the growth of applied dynamic- and predisplacement, and the distribution is high in the middle and low on the two sides. The reasons for this distribution are that the deformation of the middle part is larger than that of the two sides, and there is heat conduction between the end of the rubber column and the metal fixtures.
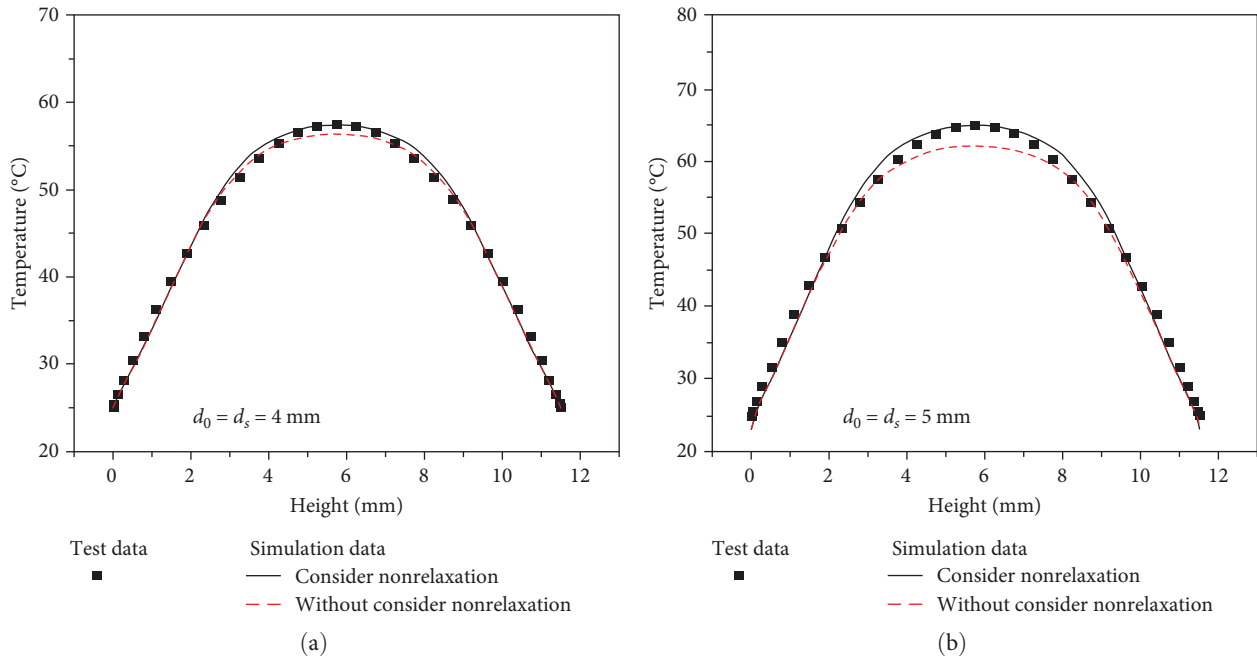
FIGURE 9: Test data and simulation data of steady-state surface temperature of rubber column: (a) $d_0 = d_s = 4$ mm; (b) $d_0 = d_s = 5$ mm.
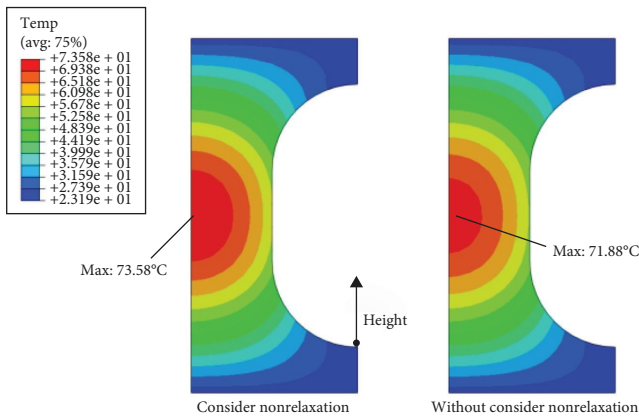

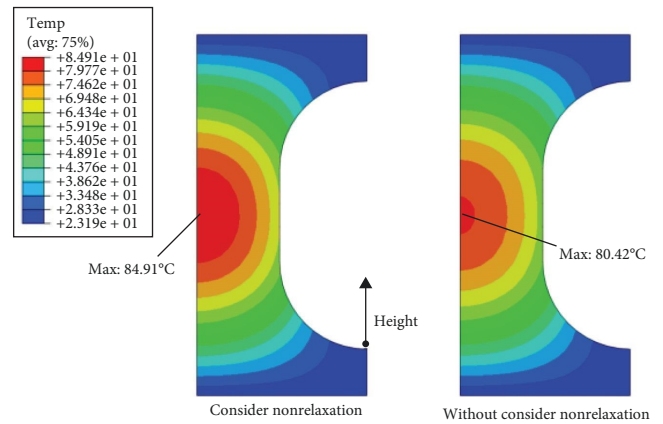FIGURE 10: Internal steady-state temperature field with $d_0 = d_s = 4$ mm.

FIGURE 11: Internal steady-state temperature field with $d_0 = d_s = 5$ mm.

The simulation results based on KMPT reach convergence (i.e., steady-state) after two iterations, and the simulation results based on the Kraus model only considering temperature reach convergence after four iterations. The simulation results of the internal steady-state temperature of rubber columns are shown in Figures 10 and 11. In all the numerical results, the temperature distribution is the same, except for the numerical difference. Because of the low thermal conductivity of the carbon black-filled rubber and the large deformation in the middle section of the rubber column, the highest temperature appears in the core of the rubber column. In Figures 10 and 11, it can be seen that the numerical result of core temperature considering nonrelaxation is higher than that without considering. With the increase of dynamic- and predisplacement, this difference of maximum

temperature becomes larger. When $d_0 = d_s = 5$ mm, the gap between the two maximum temperatures reached 5%.

Figure 9 demonstrates the comparisons between numerical results and experimental results at $d_0 = d_s = 4$ and 5 mm. These two figures reveal that the calculated results of surface temperature by accounting for the nonrelaxation agree with the measured data well; both $d_0 = d_s = 4$ and 5 mm. This good fit again verifies the reliability of KMPT. However, the numerical results without considering nonrelaxation are lower than the measured data in the middle part. As we can see in Figure 9, the deviation due to not taking into account the nonrelaxation is not obvious at $d_0 = d_s = 4$ mm; the maximum difference between the numerical and experimental results is 1.15°C, corresponding to an error of 2%. Nevertheless, when $d_0 = d_s = 5$ mm, the maximum difference

has reached 3°C, corresponding to an error of 4.6%. The comparison between Figures 9(a) and 9(b) shows that only taking temperature into consideration in HBU simulation is not accurate enough when carbon black-filled rubber is subjected to dynamic load in the nonrelaxed state. As the prestrain increases, the error caused by not considering the nonrelaxation becomes larger and larger until it cannot be ignored.

6. Conclusions

For the needs of the rubber industry, the influence of nonrelaxation on the viscoelastic properties of carbon black-filled rubber is studied. We develop an explicit model, KMPT, that can predict the storage and loss moduli well under various prestrains, temperatures, and dynamic strain amplitudes. The key to KMPT is the assumption that parameters E'_∞, $\Delta E'$, E''_∞, and $\Delta E''$ of the Kraus model increase exponentially with the prestrain ε_s. Prestrain scanning experiments at different dynamic strains and dynamic strain scanning experiments at different temperatures are carried out to determine the model parameters and verify the model. In the further verification of the KMPT, the HBU of the rubber column subjected to sinusoidal tensile displacement load is tested and simulated. The calculated results based on the KMPT are almost consistent with the infrared test data. However, the calculated results based on the model without considering nonrelaxation have a partial deviation from the measured data. As the predisplacement rises, the deviation caused without considering nonrelaxation becomes larger. In conclusion, this study is significant for rubber products subjected to vibration load in a nonrelaxed state.

Data Availability

All the data required are available within the manuscript and supplementary material.

Conflicts of Interest

The authors declare that there are no conflicts of interest.

Authors' Contributions

Xinyi Lin contributed to the writing—original draft (lead), methodology (equal), and formal analysis (equal). Mengxi Huang contributed to the investigation (equal) and methodology (equal). Yang Wang contributed to the supervision (supporting) and writing—review and editing (equal). Ziran Li contributed to the project administration (supporting), supervision (lead), and writing—review and editing (equal).

Acknowledgments

Supplementary Materials

Figures S1 and S2 show the fitting effect of the KMPT model when the prestrain correlation data are first fitted, and Table S1 lists the determined parameters. Figures S3 and S4 demonstrate the DMA test results of tire side compound and fitting effects with the KMPT model. Figure S5 shows the curve fitting of uniaxial test data for the determination of hyperelastic Yeoh model parameters. Figure S6 shows the detailed thermal boundary conditions. Table S2 lists the fitting parameters of the tire side compound. Table S3 shows the Yeoh constitutive model material parameters of the tire body compound. Table S4 demonstrates the thermal parameters in the heat conductivity analysis. (*Supplementary Materials*)

References

[1] A. R. Payne, "The dynamic properties of carbon black-loaded natural rubber vulcanizates. Part I," *Journal of Applied Polymer Science*, vol. 6, no. 19, pp. 57–63, 1962.

[2] A. R. Payne, "The dynamic properties of carbon black loaded natural rubber vulcanizates. Part II," *Journal of Applied Polymer Science*, vol. 6, no. 21, pp. 368–372, 1962.

[3] S. Bouzidi and H. Bechir, "Modeling Payne effect on basis of linearization of a visco-hyperelastic model," *Modelling and Simulation in Materials Science and Engineering*, vol. 30, no. 3, Article ID 035003, 2022.

[4] G. Huber, T. A. Vilgis, and G. Heinrich, "Universal properties in the dynamical deformation of filled rubbers," *Journal of Physics: Condensed Matter*, vol. 8, no. 29, Article ID L409, 1996.

[5] P. G. Maier and D. Göritz, "Molecular interpretation of the Payne effect," *Kautschuk Gummi Kunststoffe*, vol. 49, no. 1, pp. 18–21, 1996.

[6] A. S. Yankin, R. V. Bul'bovich, S. V. Slovikov, V. E. Vil'deman, and V. V. Pavlogradskii, "Viscoelastic characteristics of highly filled polymer composites under two-frequency actions," *Mechanics of Composite Materials*, vol. 52, pp. 81–88, 2016.

[7] G. Kraus, "Mechanical losses in carbon-black-filled rubbers," *Applied Polymer Symposia*, vol. 39, pp. 75–92, 1984.

[8] J. D. Ulmer, "Strain dependence of dynamic mechanical properties of carbon black-filled rubber compounds," *Rubber Chemistry and Technology*, vol. 69, no. 1, pp. 15–47, 1996.

[9] G. D. Dean, J. C. Duncan, and A. F. Johnson, "Determination of non-linear dynamic properties of carbon-filled rubbers," *Polymer Testing*, vol. 4, no. 2–4, pp. 225–249, 1984.

[10] A. Lion, B. Dippel, and C. Liebl, "Thermomechanical material modelling based on a hybrid free energy density depending on pressure, isochoric deformation and temperature," *International Journal of Solids and Structures*, vol. 51, no. 3-4, pp. 729–739, 2014.

[11] X. Hu, R. He, Y. Huang, B. Yin, and W. Luo, "A method to predict the dynamical behaviors of carbon black filled natural rubber at different temperatures," *Polymer Testing*, vol. 79, Article ID 106067, 2019.

[12] J. D. Ferry, "Viscoelastic properties of polymer solutions," *Journal of Research of the National Bureau of Standards*, vol. 41, pp. 53–62, 1948.

[13] A. Lion, "Thixotropic behaviour of rubber under dynamic loading histories: experiments and theory," *Journal of the Mechanics and Physics of Solids*, vol. 46, no. 5, pp. 895–930, 1998.

[14] S. Vieweg, R. Unger, K. Schroeter, E. Donth, and G. Heinrich, "Frequency and temperature dependence of the small-strain behavior of carbon-black filled vulcanizates," *Polymer Networks & Blends*, vol. 5, no. 4, pp. 199–204, 1995.

[15] A. Delattre, S. Lejeunes, F. Lacroix, and S. Méo, "On the dynamical behavior of filled rubbers at different temperatures: experimental characterization and constitutive modeling," *International Journal of Solids and Structures*, vol. 90, pp. 178–193, 2016.

[16] W. Luo, X. Hu, C. Wang, and Q. Li, "Frequency- and strain-amplitude-dependent dynamical mechanical properties and hysteresis loss of CB-filled vulcanized natural rubber," *International Journal of Mechanical Sciences*, vol. 52, no. 2, pp. 168–174, 2010.

[17] N. K. Dutta and D. K. Tripathy, "Effects of types of fillers on the molecular relaxation characteristics, dynamic mechanical, and physical properties of rubber vulcanizates," *Journal of Applied Polymer Science*, vol. 44, no. 9, pp. 1635–1648, 1992.

[18] Z. Xie, Y. T. Wei, Y. Liu, and X. Du, "Dynamic mechanical properties of aged filled rubbers," *Journal of Macromolecular Science, Part B: Physics*, vol. 43, no. 4, pp. 805–817, 2004.

[19] D. Wollscheid and A. Lion, "Predeformation- and frequency-dependent material behaviour of filler-reinforced rubber: experiments, constitutive modelling and parameter identification," *International Journal of Solids and Structures*, vol. 50, no. 9, pp. 1217–1225, 2013.

[20] J. C. Simo, "On a fully three-dimensional finite-strain viscoelastic damage model: formulation and computational aspects," *Computer Methods in Applied Mechanics and Engineering*, vol. 60, no. 2, pp. 153–173, 1987.

[21] B.-K. Kim and S.-K. Youn, "A viscoelastic constitutive model of rubber under small oscillatory load superimposed on large static deformation," *Archive of Applied Mechanics*, vol. 71, no. 11, pp. 748–763, 2001.

[22] F. S. Conant, "Tire temperatures," *Rubber Chemistry and Technology*, vol. 44, no. 2, pp. 397–439, 1971.

[23] S. K. Clark and R. N. Dodge, "Heat generation in aircraft tires under free rolling conditions," NASA Contractor Reports, 1982.

[24] D. Whicker, A. L. Browne, D. J. Segalman, and L. E. Wickliffe, "A thermomechanical approach to tire power loss modeling," *Tire Science and Technology*, vol. 9, no. 1, pp. 3–18, 1981.

[25] H. He, J. Liu, Y. Zhang et al., "Heat build-up and rolling resistance analysis of a solid tire: experimental observation and numerical simulation with thermo-mechanical coupling method," *Polymers*, vol. 14, no. 11, Article ID 2210, 2022.

[26] Z. Shida, M. Koishi, T. Kogure, and K. Kabe, "A rolling resistance simulation of tires using static finite element analysis," *Tire Science and Technology*, vol. 27, no. 2, pp. 84–105, 1999.

[27] K. Liang, Q. Tu, X. Shen et al., "Modeling and verification of rolling resistance torque of high-speed rubber track assembly considering hysteresis loss," *Polymers*, vol. 15, no. 7, Article ID 1642, 2023.

[28] J. Liu, J. Lyu, M. Shen, and F. Zhao, "Using olefin metathesis reaction to modify solution polymerized styrene-butadiene rubber (SSBR) by for a more stable "green tire"," *Journal of Polymer Research*, vol. 30, Article ID 90, 2023.

[29] F. Li, F. Liu, J. Liu et al., "Thermo-mechanical coupling analysis of transient temperature and rolling resistance for solid rubber tire: numerical simulation and experimental verification," *Composites Science and Technology*, vol. 167, pp. 404–410, 2018.

[30] J. R. Cho, H. W. Lee, W. B. Jeong, K. M. Jeong, and K. W. Kim, "Numerical estimation of rolling resistance and temperature distribution of 3-D periodic patterned tire," *International Journal of Solids and Structures*, vol. 50, no. 1, pp. 86–96, 2013.

[31] M. Rafei, M. H. R. Ghoreishy, and G. Naderi, "Computer simulation of tire rolling resistance using finite element method: effect of linear and nonlinear viscoelastic models," *Proceedings of the Institution of Mechanical Engineers, Part D: Journal of Automobile Engineering*, vol. 233, no. 11, pp. 2746–2760, 2018.

[32] A. Quek and R. Balasubramanian, "Mathematical modeling of rubber tire pyrolysis," *Journal of Analytical and Applied Pyrolysis*, vol. 95, pp. 1–13, 2012.

[33] H. Smaoui, M. Arous, H. Guermazi, S. Agnel, and A. Toureille, "Study of relaxations in epoxy polymer by thermally stimulated depolarization current (TSDC) and dielectric relaxation spectroscopy (DRS)," *Journal of Alloys and Compounds*, vol. 489, no. 2, pp. 429–436, 2010.

[34] H. Zhou, L. Song, A. Lu, T. Jiang, F. Yu, and X. Wang, "Influence of immobilized rubber on the non-linear viscoelasticity of filled silicone rubber with different interfacial interaction of silica," *RSC Advances*, vol. 6, no. 18, pp. 15155–15166, 2016.

[35] G. Heinrich and M. Klüppel, "Recent advances in the theory of filler networking in elastomers," in *Filled Elastomers Drug Delivery Systems*, vol. 160 of *Advances in Polymer Science*, pp. 1–44, Springer, Berlin, Heidelberg, 2002.

[36] S. Futamura and A. A. Goldstein, "Prediction and simulation of tire performance characteristics based on deformation index concept," *Rubber Chemistry and Technology*, vol. 89, no. 1, pp. 1–21, 2016.

[37] A. K. Bazkiaei, K. H. Shirazi, and M. Shishesaz, "Thermo-hyper-viscoelastic analysis of a rubber cylinder under cyclic deformation," *Journal of Rubber Research*, vol. 24, pp. 13–26, 2021.

[38] Q. Wang, T. Sun, C. Wei et al., "Liquid 3,4-polyisoprene: a novel processing aid to achieve tire tread SBR composites with high wet grip and low energy consumption," *Polymer Testing*, vol. 115, Article ID 107713, 2022.

[39] F. Li, J. Liu, H. Yang, Y. Lu, and L. Zhang, "Numerical simulation and experimental verification of heat build-up for rubber compounds," *Polymer*, vol. 101, pp. 199–207, 2016.

[40] O. H. Yeoh, "Some forms of the strain energy function for rubber," *Rubber Chemistry and Technology*, vol. 66, no. 5, pp. 754–771, 1993.

[41] W. Luo, B. Yin, X. Hu, Z. Zhou, Y. Deng, and K. Song, "Modeling of the heat build-up of carbon black filled rubber," *Polymer Testing*, vol. 69, pp. 116–124, 2018.

[42] B. Zhang, Y. He, and L. X. Ma, "Mechanical and thermal properties of carbon black filled natural rubber and fractal analysis of rubber fracture surfaces," in *Progress in Polymer Processing*, C. Zhang, Ed., vol. 501, pp. 479–483, Trans Tech Publications Ltd., Switzerland, 2012.